ARTICLE

Remarkable near-infrared chiroptical properties of chiral Yb, Tm and Er complexes

Received 00th January 20xx,
Accepted 00th January 20xx

DOI: 10.1039/x0xx00000x

Oliver G. Willis,[a] Francesco Zinna,*[a] Gennaro Pescitelli,[a] Cosimo Micheletti,[a] and Lorenzo Di Bari *[a]

We carried out a study of absorption (CD) and emission (CPL) chiroptical properties in the NIR region of two sets of Yb, Tm and Er complexes. The two complexes include a D_3 symmetric, $[TMG\text{-}H^+]_3Ln(BINOLate)_3$ (Ln = Yb, Tm, Er; TMG = 1,1,3,3-tetramethylguanidine; BINOLate = 1,1'-Bi-2-naphtholate), and a tetrakis, C_4 symmetric, $CsLn(hfbc)_4$ (Ln = Yb, Tm, Er; hfbc = 3-heptafluorobutylyrylcamphorate). The lanthanides studied gave access to three discrete energy domains, Yb (900-1040 nm), Tm (1180-1250 nm) and Er (1430-1600 nm) in which the chiroptical activity was assesed using g_{abs} (and g_{lum} for Yb complexes). Exceptionally high discrimination between left and right circularly polarised light was observed, with values up almost to the theoretical maximum (±2).

Introduction

In recent years, a renewed interest in the study of chiroptical properties in both absorption and emission has occurred. Compounds showing significant optical activity have applications in chiral electronics and photonics, such as circularly polarized OLEDs,[1–3] polarization sensitive phototransistors,[4] spin filters,[5] etc.[6–8] To fully exploit these possibilities, a thorough spectroscopic investigation into chiroptical properties of selected compounds is necessary, both to improve fundamental understanding and to help direct research when choosing a system for an intended application. In this context, thanks to the nature of *f-f* transitions, lanthanide complexes prove effective in displaying significant chiroptical properties.[3,9]

Beyond the UV-vis domain, where most chiroptical properties are studied, it is possible to prepare lanthanide complexes endowed with effective CD (circular dichroism) and CPL (circularly polarized luminescence) in the NIR region.[9–12] Indeed, NIR wavelengths are of high interest in view of potential applications, such as, in-vivo imaging,[13] telecommunications,[14] etc.[15] Despite the potential avenues of applications, there are only a few reports of NIR CPL, measured for Yb in the 900-1040 nm region,[1,12,16–18] and rare or even no examples of NIR CD of lanthanide complexes at lower energies available.[3,19] In general, organic chiral compounds or *d*-metal complexes show modest absorption (g_{abs}) and emission dissymmetry factors (g_{lum}), defined as:

$$g_{abs} = \frac{\Delta A}{A} = \frac{\Delta \varepsilon}{\varepsilon}, \qquad g_{lum} = \frac{\Delta I}{I}$$

With ΔA, Δε, ΔI being the differential absorption, extinction coefficient and emission intensity between left and right circularly polarized light, respectively. While the maximum value for g_{abs} is |2|, most isolated (*i.e.,* non-aggregated) chiral molecules show values around 10^{-4}-10^{-2}, while also appearing mostly in the UV or visible range.[20–24]

In this work we aim at demonstrating that selected transitions of certain chiral complexes of Yb, Tm and Er can show dissymmetry factors close to the theoretical maximum in the 900-1600 nm region. Our investigation is focused on the NIR transitions which are most likely to show strong chiroptical properties according to Richardson's theory.[25] Richardson analysed the selection rules needed to observe high optical and chiroptical activity for *f-f* transitions by considering the spin-orbit and crystal field perturbation terms required to produce non-vanishing magnetic and electric dipole transitions.[25] Accordingly, he grouped *f-f* transitions by the expected relative intensity of transition dipole moments (EI > EII > EIII > EIV), rotatory strengths (RI > RII > RIII > RIV) and dissymmetry factors (DI > DII > DIII).[25] Following this theory, we selected NIR transitions belonging to classes EI, RI and DII, namely Yb $^2F_{7/2} \leftrightarrow {}^2F_{5/2}$ (900-1040 nm), Tm $^3H_6 \rightarrow {}^3H_5$ (1190-1240 nm) and Er $^4I_{15/2} \rightarrow {}^4I_{13/2}$ (1430-1600 nm). These term-to-term transitions are zero-order magnetic dipole allowed and gain their electric dipole strength from the *ungerade* crystal field interaction term. Therefore, their absorption and CD are relatively strong and easy to measure compared to other parity-forbidden *f-f* transitions. Most importantly, the fact they belong to the DII class promises relatively high g_{abs}/g_{lum} values.

For each term-to-term transition, rich manifolds of multiple signals are expected corresponding to the various non-generate M_J levels. In a crystal field, each term is split into a theoretic maximum of 2J+1 states in a C_1 environment. In the following, the lowest level of the ground state is labelled 1, while the lowest level in the excited state is denoted as 1'. If the energy difference between various M_J levels in the ground state is

[a] Dipartimento di Chimica e Chimica Industriale, Università di Pisa, via Moruzzi 13, 56124 Pisa, Italy. E-mail: francesco.zinna@unipi.it, lorenzo.dibari@unipi.it

Electronic Supplementary Information (ESI) available: [compound preparation, additional spectral data]. See DOI: 10.1039/x0xx00000x

comparable with the thermal energy available at room temperature (k_BT at 300 K is 209 cm^{-1}), hot-bands are likely to be observed. Such components may complicate the interpretation of the spectral features observed. A similar reasoning holds for the emission spectra.

For this study, two series of lanthanide complexes with relatively symmetric and stable solution structures were chosen (Scheme 1). One set of structures involves D_3 binaphtholate (BINOLate) complexes, whose general structure was reported by Shibasaki et al in 1992.[26] To render such structure more water and air inert/stable, as proposed by Walsh *et al* in 2014, the alkali earth metal linker, such as Li^+, Na^+ and K^+ was replaced with tetramethyl guanidinium (TMG-H^+, Scheme 1).[27] Despite its chiroptical potentialities, this particular structure has not been investigated in terms of the photophysical properties, as these classes of complexes are often studied and developed in the context of catalysis.[26–29]

As a reference, chiroptical properties of C_4-symmetric $CsLn(hfbc)_4$ (hfbc = 3-heptafluorobutylyrylcamphorate, Scheme 1) were studied in the same 900-1600 nm region. These complexes are able to induce extraordinary chiroptical properties on Ln-centred *f-f* transitions, due to their almost perfect antiprism geometry which allows for effective dynamic coupling between the *f-f* and electric dipole transition moment of the π–π* transition on the diketonate moieties.[30] The best-known compound of the series is $CsEu(hfbc)_4$ showing the highest g_{lum} reported for any molecular emitter (+1.38),[31,32] while NIR-CPL for $CsYb(hfbc)_4$ has never been described. NIR-CD up to 1100 nm of the whole $CsLn(hfbc)_4$ series was investigated by Kaizaki *et al*,[9] however, lower energy term-to-term transitions, where stronger CD is expected for Tm and Er, were not reported.

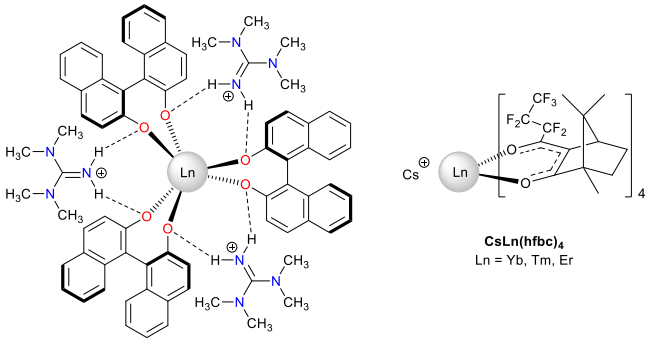

$[TMG\text{-}H^+]_3Ln(BINOLate)_3$
Ln = Yb, Tm, Er

$CsLn(hfbc)_4$
Ln = Yb, Tm, Er

Scheme 1. Structures of each set of complexes investigated in this work.

Results and discussion

NIR properties

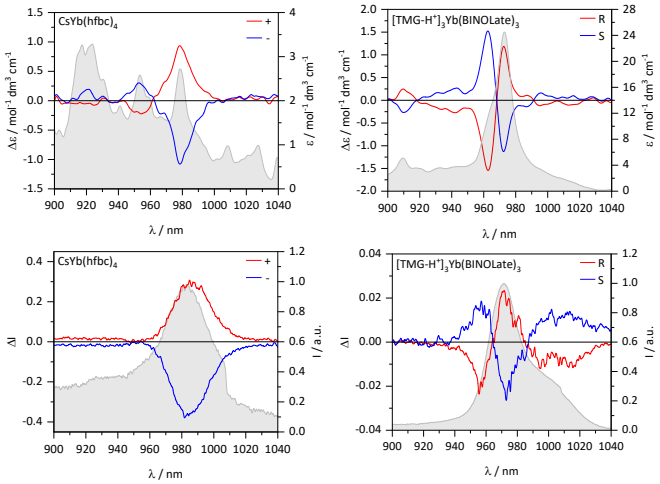

Figure 1. Top: NIR-CD spectra of $CsYb(hfbc)_4$ (4 mM) and $[TMG\text{-}H^+]_3Yb(BINOLate)_3$ (8 mM) with average total absorption traced in the background. Bottom: NIR-CPL spectra of $CsYb(hfbc)_4$ (1 mM) and $[TMG\text{-}H^+]_3Yb(BINOLate)_3$ (1 mM) with normalised average total emission traced in the background. Spectra recorded in CH_2Cl_2 at room temperature. λ_{exc} = 365 nm.

In the case of ytterbium, a single intra-configurational 4*f*-4*f* manifold, from the $^2F_{7/2}$ ground state to the $^2F_{5/2}$ excited state, is expected.[11,25] This term to term transition, falling around 970-980 nm, belongs to classes EI, RI and DII, as introduced before, according to Richardson's classification.[11] Due to the crystal field provided by the ligands, the ground and excited states are split into four and three Stark levels respectively, each of double degeneracy (Kramer's doublets).[33] The splitting between each Stark level depends on the strength of the ligand's interaction with the f-orbitals. Multiple bands can be seen within the $[TMG\text{-}H^+]_3Yb(BINOLate)_3$ spectra, with the most prominent signals occurring at 909, 962 and 972 nm. The latter, at 972 nm, is aligned with the strongest absorption signal associated with the 1→1' transition (Figure 1). Due to the various overlapping bands, a safe spectral assignment is difficult. The two strongest CD transitions, 1→1' and 1→2', show an energy difference of 107 cm^{-1}. For $CsYb(hfbc)_4$, the two lowest energy transitions at 955 and 979 nm, corresponding to the 1→1' and 1→2' have an energy gap of 256 cm^{-1}. For both complexes studied, mirror image spectra of the two enantiomers were observed. For $[TMG\text{-}H^+]_3Yb(BINOLate)_3$, the two bands from 962 to 972 nm possess a positive/negative signal sequence (for the S absolute configuration). The two bands from 955 nm to 979 nm for $CsYb(hfbc)_4$ give a similar bisignate pattern, namely, positive/negative, from lower to higher energy, for the (-)-hfbc enantiomer. The total absorption spectrum for $CsYb(hfbc)_4$ is much weaker compared to $[TMG\text{-}H^+]_3Yb(BINOLate)_3$, likely caused by the high symmetry of the coordination polyhedron of $CsLn(hfbc)_4$ complexes, which is close to an achiral regular square antiprism.[10,30,31] The extinction coefficient for CsYb(hfbc) is similar to that previously measured by Kaizaki *et al*.[9] The extinction coefficient for the $[TMG\text{-}H^+]_3Yb(BINOLate)_3$ enantiomers are also within the same order of magnitude as previously reported for similar compounds.[12] Absorption

dissymmetry factors (g_{abs}) were calculated for both complexes yielding maximal values at 983 nm of -0.46 for CsYb((-)-hfbc)$_4$ and +0.39 for CsYb((+)-hfbc)$_4$. For both [TMG-H$^+$]$_3$Yb(BINOLate)$_3$ enantiomers, maximum g_{abs} values were obtained at 962 nm with values of |0.14|. We note that the NIR-CD spectrum of [TMG-H$^+$]$_3$Yb(BINOLate)$_3$ is significantly different from the one reported for similar BINOLate compounds ([M$^+$]$_3$Yb(BINOLate)$_3$).[11] This is probably due to a different geometry of the complexes determined by the different nature of the cation.[11]

Both CsYb(hfbc)$_4$ and [TMG-H$^+$]$_3$Yb(BINOLate)$_3$ are NIR luminescent upon 365 nm irradiation. In the case of [TMG-H$^+$]$_3$Yb(BINOLate)$_3$, lanthanide emission may be sensitized via the usual triplet-Ln energy transfer, as the ligand's triplet level lies at low energy and can therefore transfer energy to Yb. Indeed, lanthanides emitting in the visible, such as Eu and Tb, cannot be sensitized by binaphtholates, as its triplet level lies below the lanthanide emissive states.[34] On the other hand, in the case of CsYb(hfbc)$_4$, where the triplet state lies much higher in energy (19760 cm^{-1}),[35] different sensitization mechanisms need to be at play, such as photo-induced electron transfer involving Yb^{3+}/Yb^{2+} species.[36] Whichever mechanism responsible, it was possible to study the NIR CPL for Yb complexes to probe the $^2F_{5/2}\rightarrow{}^2F_{7/2}$ manifold in the same 900 to 1050 nm range.

For CsYb(hfbc)$_4$, we see the same single band at 985 nm as in NIR-CD, with the transition being associated to the 1'→1 (Figure 1). As expected, g_{lum} and g_{abs} calculated around 988 nm gave similar values of -0.38 (CsYb((+)-hfbc)$_4$) and +0.31 (CsYb((-)-hfbc)$_4$) (Figure S1). To the best of our knowledge, this dissymmetry factor value in emission is the highest for any molecular species emitting within the range of 900 to 1050 nm.[1,12,16–18,37] The observed sign also matches in both absorption and emission.

In the case of the [TMG-H$^+$]$_3$Yb(BINOLate)$_3$ complex, several CPL signals with varying signs are present compared to the NIR-CPL spectrum of CsYb(hfbc)$_4$. The two signals of [TMG-H$^+$]$_3$Yb(BINOLate)$_3$, occurring at 957 and 975 nm, are aligned with the two major bands seen in CD, while also bearing the same sign (Figure 1). While the most intense signal at 975 nm may be associated to the 1'→1 transition, the higher energy band at 957 nm is likely stemming from the 2'→1.

Comparing g_{abs} and g_{lum} of [TMG-H$^+$]$_3$Yb(BINOLate)$_3$, we see a large decrease in the polarisation degree, from a maximum of |0.14| (g_{abs} at 962 nm) to |0.066| (g_{lum} at 954 nm). This may be rationalized by the fact that for close or overlapping transitions with opposite signs, partial signal cancellation may occur.[10,12] This means that a quantitative comparison between emission and absorption dissymmetry factors is not straightforward.

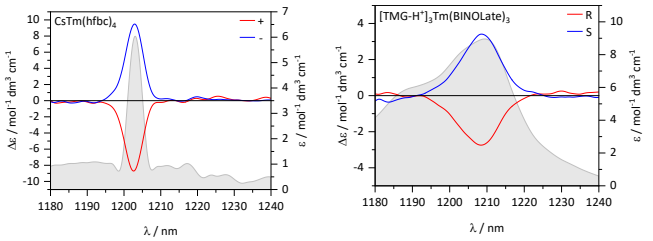

Figure 2. NIR-CD spectra of CsTm(hfbc)$_4$ (4 mM) and [TMG-H$^+$]$_3$Tm(BINOLate)$_3$ (10 mM) with average total absorption traced in the background. Spectra recorded in CH_2Cl_2 at room temperature.

Contrary to Yb^{3+}, Tm^{3+} has several term-to-term transitions arising from the $^3H_6$ ground state.[25,32] We focused on the $^3H_6\rightarrow{}^3H_5$ manifold occurring around 1210 nm, which belongs to the DII class and therefore a considerable CD signal is expected. Despite the numerous amount of non-degenerate M$_J$ sublevels, even in a relatively high symmetry environment, in both complexes a single, monosignate, intense absorption and CD band is observed at 1203 and 1209 nm, for CsTm(hfbc)$_4$ and [TMG-H$^+$]$_3$Tm(BINOLate)$_3$ respectively (Figure 2). This is in line with what has already been observed by our group for C$_1$-symmetrical Tm diketonates.[38] Although it is still not clear the reason behind such constructive overlap of transitions, this process may lead to remarkably high dissymmetry factors.

The [TMG-H$^+$]$_3$Tm(BINOLate)$_3$ spectrum contains an extra absorption band at higher energy with no associated CD signal. In order to check for possible ligand vibrational overtones falling in this spectral range, the absorption spectrum of [TMG-H$^+$]$_3$La(BINOLate)$_3$ was measured and showed no absorption contribution from the ligands within the 1180-1250 nm region (Figure S2). In this case, compared to the ytterbium analogues, both complexes have similar extinction coefficients, however the CD signal for CsTm(hfbc)$_4$ is more than twice that of [TMG-H$^+$]$_3$Tm(BINOLate)$_3$. The monosignate signals also have contrasting linewidths despite being measured using the same experimental conditions. Indeed, the FWHM for CsTm(hfbc)$_4$ is 5.5 nm, while for [TMG-H$^+$]$_3$Tm(BINOLate)$_3$ it is more than double at 13 nm. The cause of the different signal widths may be related to the crystal field strengths in the two complexes. Another key observation is that the [TMG-H$^+$]$_3$Tm(BINOLate)$_3$ absorption band is red-shifted with respect to the CsTm(hfbc)$_4$ signal. The g_{abs} values at 1208 nm for [TMG-H$^+$]$_3$Tm(BINOLate)$_3$ are +0.38 and -0.31 for the S and R enantiomers respectively. For CsTm(hfbc)$_4$, the dissymmetry factor values reach up to the theoretical maximum, indicating almost complete selective absorption of either right- or left-circularly polarized light.

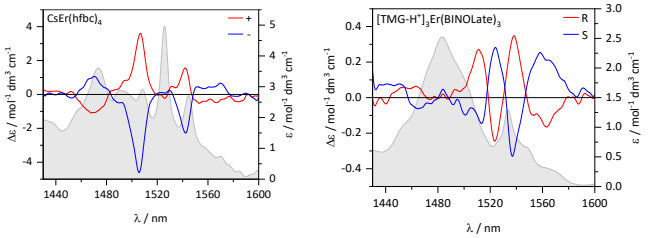

Figure 3. NIR-CD spectra of CsEr(hfbc)$_4$ (3 mM) and [TMG-H$^+$]$_3$Er(BINOLate)$_3$ (17 mM) with average total absorption traced in the background. Spectra recorded in $CDCl_3$ at room temperature.

In the case of Er, we focused on the $^4I_{15/2} \rightarrow {}^4I_{13/2}$ manifold, falling between 1430 and 1600 nm.[25,32] Such term-to-term transition belongs to the same Richardson classes as with Yb and Tm. It is therefore a promising manifold to show strong chiroptical properties with high dissymmetry factors. Surprisingly, to the best of our knowledge, its CD has never been reported so far.

The complete spectral assignments for these two complexes are made difficult by the various bands observed which overlap and partially cancel out. Given the spin-orbit coupling values of 15/2 and 13/2, in a non-cubic environment, each term is split into 8 and 7 sub-levels respectively, with a maximum number of 56 components possible (including hot bands).[33] For both complexes, strong CD signals are observed, occurring at varying wavelengths (Figure 3). The most intense absorption band for $CsEr(hfbc)_4$ at 1526 nm has no associated CD signal. As with the $[TMG\text{-}H^+]_3Tm(BINOLate)_3$ complex, the absorption spectra of $[TMG\text{-}H^+]_3La(BINOLate)_3$ was measured within this region (Figure S2). The $[TMG\text{-}H^+]_3La(BINOLate)_3$ absorption spectrum showed one signal occurring at 1454 nm, which can be seen as the shoulder on the most intense band for $[TMG\text{-}H^+]_3Er(BINOLate)_3$. In this case, some significant contributions to absorption from ligand vibrational overtones are present (in particular at 1453 and 1532 nm), therefore g_{abs} calculated for those bands are likely underestimated. As foreseen, in both cases, the dissymmetry factors are exceptionally large, and indeed larger than the analogous Yb complexes. $[TMG\text{-}H^+]_3Er(BINOLate)_3$ shows g_{abs} of +0.26/-0.15, -0.34/+0.40 and +0.40/-0.32 at 1514, 1524 and 1539 nm for the R/S enantiomers, while $CsEr(hfbc)_4$ displays even higher values, namely +1.31/-1.70 and +0.71/-1.02 at 1506 and 1541 nm for the(+)/(-) hfbc absolute configurations (see Figure 4). We remark that such Er band is of particular practical interest, as it falls within two regions of the silica optical telecommunications window, the S-band (1460 – 1530 nm) and C- band (1530 – 1565 nm).[39,40]

Figure 4 shows the g_{abs}-*vs*-wavelength plots for the two series of Yb, Tm and Er complexes investigated in this work.

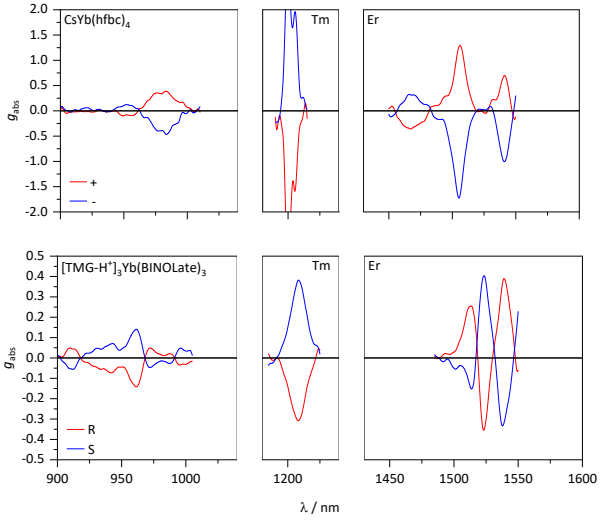

Figure 4. Top: g_{abs}-*vs*-wavelength plot for $CsLn(hfbc)_4$ (Ln = Yb, Tm, Er). Bottom: g_{abs}-*vs*-wavelength plot for $[TMG\text{-}H^+]_3Ln(BINOLate)_3$ (Ln = Yb, Tm, Er).

Compound structure

The solution structure of $CsLn(hfbc)_4$ series were previously determined through paramagnetic NMR.[30] Such structure shows an almost perfect C_4 antiprism geometry. On the other hand, an X-ray structure for $[TMG\text{-}H^+]_3Yb(BINOLate)_3$, showing a D_3 geometry, was reported by Walsh *et al.*[27] In order to look for any differences between solid state and solution ($CDCl_3$) structures, an analysis of NMR pseudo-contact shift and longitudinal relaxation rate (ρ_1) was carried out.[41] The NMR spectrum of $[TMG\text{-}H^+]_3Yb(BINOLate)_3$ is compatible with a D_3 geometry, moreover the distance between each H atom and Yb-centre (r), estimated from the relaxation rates ρ_1 ($\rho_1 \propto 1/r^6$) is in agreement with the solid state structure (Figure S1).[27] On the other hand, the paramagnetic shifts are not in agreement with the geometrical factors calculated from the X-ray structures (Figure S2),[41] this would indicate a rearrangement of the ligands around the metal centre upon complex dissolution. For all data described above, see Table S1.

Because of the well-known sensitivity of CD to the binaphthyl structure,[42,43] we completed the chiroptical investigations into the $[TMG\text{-}H^+]_3Ln(BINOLate)_3$ class of compound by recording the CD spectra within the range of 210 to 450 nm. The absorption and CD spectra of the Yb, Tm and Er complexes are all consistent with each other, indicating substantial isostructurality along the series.[11]

Conclusions

The chiroptical data of two sets of relatively stable lanthanide complexes were successfully measured in a wide and exotic wavelength domain, from 900 to 1600 nm.

The transitions observed showed strong optical activity, in agreement with predictions derived from Richardson's theory.[25]

The ytterbium set of complexes showed rich chiroptical features both in absorption and emission, arising from the Stark splitting of the $^2F_{7/2} \rightarrow {}^2F_{5/2}$ manifold.

The chiroptical data of the thulium complexes showed a unique constructive addition of all possible manifold components, leading to g_{abs} factors close to the theoretical maximum.

The complexes of erbium showed remarkably rich features, partnered with large dissymmetry factors. To the best of our knowledge, no NIR CD within the range of 1430-1600 nm has been measured. These complexes also showed exceptional g_{abs} values, up to |1.70| for $CsEr(hfbc)_4$ |0.40| for the $[TMG\text{-}H^+]_3Er(BINOLate)_3$ complex. As in general, emission can be observed from this Er bands, our findings put Er as a good candidate to observe NIR-CPL in an extreme wavelength region, which is of particular interest for the fibre-optic telecommunication industry.

Conflicts of interest

There are no conflicts to declare

Acknowledgements

This project has received funding from the European Union's Horizon 2020 Research and Innovation Programme under the Marie Sklodowska-Curie grant agreement No. 859752 and from the Italian Ministero dell'Università PRIN 20172M3K5N. FZ acknowledges financial support from the University of Pisa (PRA 2020_21).

Notes and references

1 J. R. Brandt, F. Salerno and M. J. Fuchter, *Nat. Rev. Chem.*, 2017, **1**, 1–12.

2 Y. Yang, R. C. Da Costa, D. M. Smilgies, A. J. Campbell and M. J. Fuchter, *Adv. Mater.*, 2013, **25**, 2624–2628.

3 F. Zinna, U. Giovanella and L. Di Bari, *Adv. Mater.*, 2015, **27**, 1791–1795.

4 B. L. Feringa, *Acc. Chem. Res.*, 2001, **34**, 504–513.

5 R. Farshchi, M. Ramsteiner, J. Herfort, A. Tahraoui and H. T. Grahn, *Appl. Phys. Lett.*, , DOI:10.1063/1.3582917.

6 C. Wang, H. Fei, Y. Qiu, Y. Yang, Z. Wei, Y. Tian, Y. Chen and Y. Zhao, *Appl. Phys. Lett.*, 1999, **74**, 19–21.

7 C. Wagenknecht, C. M. Li, A. Reingruber, X. H. Bao, A. Goebel, Y. A. Chen, Q. Zhang, K. Chen and J. W. Pan, *Nat. Photonics*, 2010, **4**, 549–552.

8 W. B. Sparks, J. H. Hough, L. Kolokolova, T. A. Germer, F. Chen, S. DasSarma, P. DasSarma, F. T. Robb, N. Manset, I. N. Reid, F. D. Macchetto and W. Martin, *J. Quant. Spectrosc. Radiat. Transf.*, 2009, **110**, 1771–1779.

9 D. Shirotani, H. Sato, K. Yamanari and S. Kaizaki, *Dalt. Trans.*, 2012, **41**, 10557–10567.

10 F. Zinna, L. Arrico and L. Di Bari, *Chem. Commun.*, 2019, **55**, 6607–6609.

11 L. Di Bari, M. Lelli, G. Pintacuda, G. Pescitelli, F. Marchetti and P. Salvadori, *J. Am. Chem. Soc.*, 2003, **125**, 5549–5558.

12 C. L. Maupin, R. S. Dickins, L. G. Govenlock, C. E. Mathieu, D. Parker, J. A. Gareth Williams and J. P. Riehl, *J. Phys. Chem. A*, 2000, **104**, 6709–6717.

13 R. Carr, N. H. Evans and D. Parker, *Chem. Soc. Rev.*, 2012, **41**, 7673–7686.

14 H. Kim, K. Jung, S. J. Yeo, W. Chang, J. J. Kim, K. Lee, Y. D. Kim, I. K. Han and S. Joon Kwon, *Nanoscale*, 2018, **10**, 21275–21283.

15 F. Zinna and L. Di Bari, *Chirality*, 2015, **27**, 1–13.

16 F. Gendron, S. Di Pietro, L. Abad Galán, F. Riobé, V. Placide, L. Guy, F. Zinna, L. Di Bari, A. Bensalah-Ledoux, Y. Guyot, G. Pilet, F. Pointillart, B. Baguenard, S. Guy, O. Cador, O. Maury and B. Le Guennic, *Inorg. Chem. Front.*, 2021, **8**, 914–926.

17 R. S. Dickins, J. A. K. Howard, C. L. Maupin, J. M. Moloney, D. Parker, J. P. Riehl, G. Siligardi and J. A. G. Williams, *Chem. - A Eur. J.*, 1999, **5**, 1095–1105.

18 C. L. Maupin, D. Parker, J. A. G. Williams and J. P. Riehl, *J. Am. Chem. Soc.*, 1998, **120**, 10563–10564.

19 B. Lefeuvre, C. A. Mattei, J. F. Gonzalez, F. Gendron, V. Dorcet, F. Riobé, C. Lalli, B. Le Guennic, O. Cador, O. Maury, S. Guy, A. Bensalah-Ledoux, B. Baguenard and F. Pointillart, *Chem. - A Eur. J.*, 2021, **27**, 7362–7366.

20 E. M. Sánchez-Carnerero, A. R. Agarrabeitia, F. Moreno, B. L. Maroto, G. Muller, M. J. Ortiz and S. De La Moya, *Chem. - A Eur. J.*, 2015, **21**, 13488–13500.

21 J. Li, C. Hou, C. Huang, S. Xu, X. Peng, Q. Qi, W.-Y. Lai and W. Huang, *Research*, 2020, **2020**, 1–10.

22 K. Ma, W. Chen, T. Jiao, X. Jin, Y. Sang, D. Yang, J. Zhou, M. Liu and P. Duan, *Chem. Sci.*, 2019, **10**, 6821–6827.

23 W. L. Zhao, M. Li, H. Y. Lu and C. F. Chen, *Chem. Commun.*, 2019, **55**, 13793–13803.

24 Y. Nagata and T. Mori, *Front. Chem.*, 2020, **8**, 1–6.

25 F. S. Richardson, *Inorg. Chem.*, 1980, **19**, 2806–2812.

26 H. Sasai, T. Suzuki, S. Arai, T. Arai and M. Shibasaki, *J. Am. Chem. Soc.*, 1992, **114**, 4418–4420.

27 J. R. Robinson, X. Fan, J. Yadav, P. J. Carroll, A. J. Wooten, M. A. Pericàs, E. J. Schelter and P. J. Walsh, *J. Am. Chem. Soc.*, 2014, **136**, 8034–8041.

28 Z. Liu, T. Takeuchi, R. Pluta, F. Arteaga Arteaga, N. Kumagai and M. Shibasaki, *Org. Lett.*, 2017, **19**, 710–713.

29 H. C. Aspinall, J. F. Bickley, J. L. M. Dwyer, N. Greeves, R. V. Kelly and A. Steiner, *Organometallics*, 2000, **19**, 5416–5423.

30 S. Di Pietro and L. Di Bari, *Inorg. Chem.*, 2012, **51**, 12007–12014.

31 J. L. Lunkley, D. Shirotani, K. Yamanari, S. Kaizaki and G. Muller, *J. Am. Chem. Soc.*, 2008, **130**, 13814–13815.

32 J. L. Lunkley, D. Shirotani, K. Yamanari, S. Kaizaki and G. Muller, *Inorg. Chem.*, 2011, **50**, 12724–12732.

33 J.-C. G. Bünzli and S. V. Eliseeva, Springer-Verlag, 2010, pp. 1–45.

34 M. Deng, N. D. Schley and G. Ung, *Chem. Commun.*, 2020, **56**, 14813–14816.

35 F. Zinna, M. Pasini, F. Galeotti, C. Botta, L. Di Bari and U. Giovanella, *Adv. Funct. Mater.*, 2017, **27**, 1603719.

36 W. D. Horrocks, J. P. Bolender, W. D. Smith and R. M. Supkowski, *J. Am. Chem. Soc.*, 1997, **119**, 5972–5973.

37 L. Arrico, L. Di Bari and F. Zinna, *Chem. - A Eur. J.*, 2021, 27, 2920–2934.

38 M. Górecki, L. Carpita, L. Arrico, F. Zinna and L. Di Bari, *Dalt. Trans.*, 2018, **47**, 7166–7177.

39 C. B. C-band, S. Yamashita and M. Nishihara, *IEEE J. Sel. Top. Quantum Electron.*, 2001, **7**, 41–43.

40 C. H. Yeh, C. C. Lee and S. Chi, *IEEE Photonics Technol. Lett.*, 2003, **15**, 1053–1054.

41 L. Di Bari and P. Salvadori, *Coord. Chem. Rev.*, 2005, 249, 2854–2879.

42 L. Di Bari, G. Pescitelli and P. Salvadori, *J. Am. Chem. Soc.*, 1999, **121**, 7998–8004.

43 S. F. Mason, R. H. Seal and D. R. Roberts, *Tetrahedron*, 1974, **30**, 1671–1682.